# FORMATION STRESS ESTIMATION USING STANDARD ACOUSTIC LOGGING

Xiaojun Huang

Earth Resources Laboratory
Department of Earth, Atmospheric, and Planetary Sciences
Massachusetts Institute of Technology
Cambridge, MA 02139

Bikash K. Sinha

Schlumberger-Doll Research
Old Quarry Road
Ridgefield, CT 06877

M. Nafi Toksöz and Daniel R. Burns

Earth Resources Laboratory
Department of Earth, Atmospheric, and Planetary Sciences
Massachusetts Institute of Technology
Cambridge, MA 02139

## ABSTRACT

*In situ* formation stress directions and magnitudes are estimated by inverting the borehole flexural and Stoneley dispersions obtained from standard acoustic logging data (dipole and monopole logs). The underlying procedure consists of the following steps: first, we locate stressed zones in the formation by searching for crossovers in flexural dispersions. Second, the fast shear direction is estimated from the cross-dipole waveforms. It corresponds to the direction of the maximum horizontal stress ($S_H$). Finally, a multi-frequency inversion of both the Stoneley and flexural dispersions yields the maximum ($S_H$) and minimum ($S_h$) horizontal stress magnitudes together with the three formation nonlinear elastic constants, $c_{111}$, $c_{112}$ and $c_{123}$, defined about the selected reference (isotropic) state. The inversion method is based on equations that relate $S_H$ and $S_h$ with variations in phase velocities of the borehole flexural and Stoneley waves

in the stressed state from those in the assumed reference state, the state that is hydrostatically loaded and isotropic. Phase velocities of the borehole flexural and Stoneley modes as a function of frequency can be obtained from processing the cross-dipole and monopole waveforms, respectively. The borehole flexural and Stoneley dispersions in the assumed reference (isotropic) state are obtained from the solution of a standard boundary-value problem. The sensitivity functions for the inversion model are obtained from the eigenfunctions of the boundary-value problem in the reference state. Results for the stress directions and magnitudes obtained from the inversion of the Stoneley and flexural dispersions over a selected bandwidth are consistent with focal mechanism and borehole breakout data present in the world map database (Zoback, 1992).

## INTRODUCTION

Detailed knowledge of formation stress state would aid in planning stimulation treatments for enhanced recovery of hydrocarbons, prevention of sand production and borehole instability. The formation stress state at a given location can be completely characterized by magnitudes and directions of three principal stresses, $S_v$, $S_H$, and $S_h$, denoting the vertical, maximum horizontal and minimum horizontal stresses, respectively (Zoback and Zoback, 1980; Zoback, 1992). Currently, borehole breakout analysis is the most commonly used technique to estimate formation stresses. However, borehole breakouts are destructive processes that oil companies wish to avoid, because they represent shear failure of the borehole wall centered in the $S_h$ direction, the azimuth of the maximum circumferential compressive stress (Gough and Bell, 1982; Zoback *et al.*, 1985). In addition, without shear failure, this technique will fail to determine the *in situ* stress even when there is a stress concentration around the borehole.

In this paper, a nondestructive technique is described that can reliably estimate the *in situ* state of stresses in boreholes from borehole sonic measurements. Sinha and Kostek (1996) predicted in theory that a crossover in flexural dispersions is an indicator of stress-induced anisotropy dominating over other sources of intrinsic anisotropy. These predictions were subsequently verified in a scaled-borehole experiment (Winkler *et al.*, 1998. Therefore, highly stressed zones can be identified by a search of crossovers in flexural dispersions. In a stressed zone, the polarization direction of fast shear estimated from cross-dipole waveforms corresponds to the direction of the maximum horizontal stress. The direction of minimum horizontal stress is perpendicular to the fast shear direction. In the presence of horizontal stresses, $S_H$ and $S_h$, changes in the Stoneley and flexural dispersions from a nearby reference state can be described by a linear perturbation model. This perturbation model can serve as the basis for the inversion of borehole dispersions for the stress magnitudes above and beyond the stresses assumed in the hydrostatically loaded reference state of the rock (Sinha, 1997). Following the theorem of linear superposition, we derive equations that relate $S_H$, $S_h$, and the formation nonlinear elastic constants $c_{111}$, $c_{112}$ and $c_{123}$ to variations in flexural and Stoneley dispersions. A multi-frequency inversion technique based on these equations yields the

deviatoric stress magnitudes ($S_H$ and $S_h$) from those assumed in the reference state.

## STRESS MAGNITUDE ESTIMATION

To evaluate magnitudes of horizontal stresses, a perturbation model is applied that quantitatively describes how the magnitude of horizontal stresses is related to borehole flexural dispersions (Tiersten, 1978; Norris *et al.,* 1994; Sinha and Kostek, 1996).

Before we outline the perturbation derivation for a small dynamic field superimposed on a prestress, we briefly introduce some preliminary terminology and notation. The kinematics of deformation of a material point associated with a propagating wave in a stressed medium can be described in terms of three different configurations of the solid: the *reference, intermediate,* and *current* configurations of material points. These configurations denote the undeformed state, statically deformed biasing state, and the state of elastic wave-induced deformation superimposed on the bias, respectively. We first note that under the static bias the material points move from the *reference* coordinates $X_L$ to the *intermediate* coordinates $\xi_\alpha$, and we can map points from the *reference* coordinates to the *intermediate* coordinates by

$$\xi_\alpha = \xi_\alpha(X_L). \tag{1}$$

Then, for the superposed small dynamic motion, the material points move from the *intermediate* coordinates $\xi_\alpha$ to the *present* coordinates $y_i$, and we have

$$y_i = y_i(\xi_\alpha, t) = \hat{y}_i(X_L, t). \tag{2}$$

All notations follow the convention that capital Latin indices, lower-case Greek indices, and lower-case Latin indices, refer to the Cartesian components of the *reference* coordinates, *intermediate* coordinates, and *present* coordinates of material points, respectively. A comma followed by an index denotes partial differentiation with respect to a geometric coordinate. Also, the summation convention for repeated tensor indices and the dot notation for differentiation with respect to time hold here. The coordinate system is set up as $X_1$ along borehole axis, and $X_2$ and $X_3$ in the plane perpendicular to $X_1$. Equations (1) and (2) are mapping functions that relate three configurations of the solid. In this paper, the mass density, linear moduli and nonlinear moduli of the material refer to a specific *reference* state.

In a reference state, the equations of motion for a borehole mode can be expressed as

$$K^{Lm}_{L\gamma,L} + \rho_o \omega_m^2 u^m_\gamma = 0 \tag{3}$$

where $K^{Lm}_{L\gamma}$ is the Poila-Kirchhoff stress tensor in linear elasticity that defines stresses in the *intermediate* and *reference* configurations (Truesdell and Noll, 1992), $\rho_0$ is the mass density in the reference configuration, and $u^m_\gamma$ denotes a small amplitude dynamic solution to the wave equation of a fluid-filled borehole surrounded by an isotropic and homogeneous formation (*reference* state) at a harmonic frequency, $\omega_m$ (Biot, 1952).

Piola-Kirchhoff stress tensors define stresses in the *intermediate* and *reference* configurations (Truesdell, 1992).

Referring to the *reference* state, the equation of motion in the presence of initial stresses in the medium (i.e., a static bias) may be written in terms of Piola-Kirchhoff stress tensor as

$$K^L_{L\gamma,L} + K^{NL}_{L\gamma,L} + \rho_0\omega^2 u_\gamma = 0 \tag{4}$$

where $K^{NL}_{L\gamma}$ is the nonlinear portion of the Piola-Kirchhoff stress tensor that denotes the perturbation from the linear portion, $K^L_{L\gamma}$. $K^L_{L\gamma}$ and $K^{NL}_{L\gamma}$ may be expressed as

$$K^L_{L\gamma} = c_{L\gamma M\nu} u_{\nu,M} \tag{5}$$

and

$$K^{NL}_{L\gamma} = \hat{c}_{L\gamma M\nu} u_{\nu,M} \tag{6}$$

where

$$\hat{c}_{L\gamma M\nu} = T_{LM}\delta_{\gamma\nu} + c_{L\gamma M\nu AB}E_{AB} + c_{L\gamma KM}w_{\nu,K} + c_{LKM\nu}w_{\gamma,K} \tag{7}$$

with

$$T_{LM} = c_{LMRS}w_{R,S} \tag{8}$$

and

$$E_{AB} = \frac{1}{2}(w_{A,B} + w_{B,A}). \tag{9}$$

In equation (4), $u_\gamma$ denotes the small-amplitude dynamic solution at a harmonic frequency of $\omega$ in the presence of a static bias. $c_{L\gamma M\nu}$ and $c_{L\gamma M\nu AB}$ are the second and third-order elastic constants, respectively (Thurston and Brugger, 1964). In equations (7), (8) and (9), $T_{LM}$, $E_{AB}$ and $w_{\gamma,K}$ denote the biasing stresses, strains and (static) displacement gradients, respectively. Note that the biasing stresses, strains and displacement gradients are spatially varying due to borehole stress concentration; therefore, $K^L_{L\gamma,L}$ and $K^{NL}_{L\gamma,L}$ are position dependent and a direct solution of the boundary-value problem is not possible.

Equations (3) and (4) can be combined to form an integral equation valid for a continuum of arbitrary volume $V_0$ in the reference configuration:

$$\int_{V_0} dV_0[(K^L_{L\gamma,L} + K^{NL}_{L\gamma,L} + \rho_0\omega^2 u_\gamma)u^{m*}_\gamma - (K^{Lm}_{L\gamma,L} + \rho_0\omega^2_m u^m_\gamma)u^*_\gamma] = 0 \tag{10}$$

where * denotes complex conjugate. According to Guass's theorem of divergence, equation (10) can be recast into a form that is convenient for calculating a small perturbation at the frequency $\omega_m$:

$$\begin{aligned}\int_{V_0} dV_0\rho_0(\omega^2 u_\gamma u^{m*}_\gamma - \omega^2_m u^m_\gamma u^*_\gamma) &= \oint_{S_0} N_L[K^{Lm}_{L\gamma}u^*_\gamma - K^L_{L\gamma}u^{m*}_\gamma] \\ &- \int_{V_0} dV_0 K^{NL}_{L\gamma,L}u^{m*}_\gamma\end{aligned} \tag{11}$$

where $N_L$ is the outward unit normal in the reference or undeformed configuration. $S_0$ is the surface surrounding $V_0$. The quantities in the perturbed state (i.e. in the presence of biasing stresses and strains) are related to those in the unperturbed state by assuming the linear relationships

$$u_\gamma = u_\gamma^m + \epsilon u_\gamma \,, \tag{12}$$

$$u_\gamma^* = u_\gamma^* + \epsilon u_\gamma^* \tag{13}$$

and

$$\omega = \omega_m + \Delta\omega_m \tag{14}$$

where $\epsilon$ is an arbitrary small number. Substituting equation (12), (13) and (14) into equation (11) and neglecting quadratic or higher terms of $\epsilon$ and $\Delta\omega_m$ yields a general form of the perturbation integral for calculating changes in the eigenfrequency $\omega_m$ caused by the biasing stresses and strains:

$$\Delta\omega_m = \frac{\oint_{S_0} dS_0 N_L [K_{L\gamma}^{Lm} u_\gamma^* - K_{L\gamma}^{L} u_\gamma^{m*}] - \int_{V_0} dV_0 K_{L\gamma,L}^{NL} u_\gamma^{m*}}{2\omega_m \int_{V_0} \rho_0 u_\gamma^m u_\gamma^{m*} dV_0}. \tag{15}$$

The boundary surface $S_0$ is at the borehole wall; therefore, $N_L$ denotes the negative radial direction, and $N_L K_{L\gamma} u_\gamma^*$ represents the energy flux in the negative radial direction. There is no energy flow in the radial direction for any guided mode that decays away from the borehole in both the unperturbed and perturbed states. Consequently, we have

$$N_L K_{L\gamma}^{Lm} u_\gamma^{m*} = 0 \,, \tag{16}$$

and in the perturbed state we have

$$N_L (K_{L\gamma}^{L} + K_{L\gamma}^{NL}) u_\gamma^* = 0. \tag{17}$$

Applying Guass's theorem of divergence to the volume integral in the numerator of equation (15) and incorporating equations (16) and (17), the first-order perturbation in the eigenfrequency $\omega_m$ is obtained

$$\Delta\omega_m = \frac{\int_{V_0} K_{L\gamma}^{NL} u_{\gamma,L}^{m*} dV_0}{2\omega_m \int_{V_0} \rho_0 u_\gamma^m u_\gamma^{m*} dV_0}. \tag{18}$$

Note that elements of the nonlinear part of the Piola-Kirchhoff stress tensor $K_{L\gamma}^{NL}$ in equation (18) are completely known in terms of the second- and third-order elastic constants and biasing stresses in the statically deformed state as given by equations (7), (8) and (9). The index $m$ refers to the family of normal modes for a borehole in the reference state. For each of the modes that are sensitive to stress application, such as the flexural mode and Stoneley mode, at a given wavenumber $k_z$, the first-order perturbation in the eigenfrequency $\omega_m$ is estimated with the perturbation procedure.

Without reducing generality, let us assume $S_H$ is applied in the $X_2$-direction while $S_h$ is applied in the $X_3$-direction. First, let us assume only $S_H$ is present, i.e., $S_h = 0$. Thus, the borehole is subject to a uniaxial stress $S_H$. For a given eigenfrequency $\omega_m$, a first-order perturbation in eigenfrequencies of the Stoneley and flexural modes, $\omega_2$, $\omega_3$ and $\omega_{St}$, may be given by (Sinha, 1997)

$$\frac{\Delta\omega_2^H}{\omega_m} = C_1^0 S_H + C_2^0 S_H \frac{c_{111}}{c_{66}} + C_3^0 S_H \frac{c_{112}}{c_{66}} + C_4^0 S_H \frac{c_{123}}{c_{66}}, \tag{19}$$

$$\frac{\Delta\omega_3^H}{\omega_m} = C_1^{90} S_H + C_2^{90} S_H \frac{c_{111}}{c_{66}} + C_3^{90} S_H \frac{c_{112}}{c_{66}} + C_4^{90} S_H \frac{c_{123}}{c_{66}}, \tag{20}$$

and

$$\frac{\Delta\omega_{St}}{\omega_m} = C_1 S_H + C_2 S_H \frac{c_{111}}{c_{66}} + C_3 S_H \frac{c_{112}}{c_{66}} + C_4 S_H \frac{c_{123}}{c_{66}}, \tag{21}$$

where $\Delta\omega_{St}^H$, $\Delta\omega_2^H$ and $\Delta\omega_3^H$ denote first-order frequency perturbations for the Stoneley wave and flexural waves polarized in the $X_2$- and $X_3$-directions, respectively. Coefficients $C_i^0$, $C_i^{90}$, and $C_i$, with $i = 1$, 2, 3 and 4, are frequency dependent integrals that can be evaluated in terms of the known flexural wave solution in the reference state and biasing stresses of unit-magnitude and corresponding strains in the formation (see Appendix). The superscript 0 denotes flexural wave polarization along the far-field uniaxial stress direction, while 90 denotes flexural wave polarization in the perpendicular direction.

Similarly, if only $S_h$ is applied, the corresponding first-order perturbations in respective eigenfrequencies $\omega_2$, $\omega_3$ and $\omega_{St}$ are

$$\frac{\Delta\omega_2^h}{\omega_m} = C_1^{90} S_h + C_2^{90} S_h \frac{c_{111}}{c_{66}} + C_3^{90} S_h \frac{c_{112}}{c_{66}} + C_4^{90} S_h \frac{c_{123}}{c_{66}}, \tag{22}$$

$$\frac{\Delta\omega_3^h}{\omega_m} = C_1^0 S_h + C_2^0 S_h \frac{c_{111}}{c_{66}} + C_3^0 S_h \frac{c_{112}}{c_{66}} + C_4^0 S_h \frac{c_{123}}{c_{66}}, \tag{23}$$

and

$$\frac{\Delta\omega_{St}^h}{\omega_m} = C_1 S_h + C_2 S_h \frac{c_{111}}{c_{66}} + C_3 S_h \frac{c_{112}}{c_{66}} + C_4 S_h \frac{c_{123}}{c_{66}}. \tag{24}$$

Note that $S_h$ is in the $X_3$-direction; thus flexural wave polarization oriented in the $X_2$-direction is perpendicular to the far-field uniaxial stress direction. Note that first-order perturbations in the respective eigenfrequencies are linear function of stress magnitude. The total first-order frequency perturbations due to the application of the two uniaxial stresses of $S_H$ and $S_h$ are linear combinations of $\Delta\omega_m^H$ and $\Delta\omega_m^h$, i.e., $\Delta\omega_m = \Delta\omega_m^H + \Delta\omega_m^h$, with $m = 2, 3$ and $St$, respectively. Frequency perturbations $\Delta\omega_m$ are added to their respective eigenfrequencies $\omega_m$ for various values of the wavenumber along the borehole axis, $k_z$, to obtain changes in phase velocities of two principal flexural waves and the Stoneley wave at a given frequency,

$$\begin{aligned}\frac{v_2 - v_R}{v_R} = \; & S_H(C_1^0 + C_2^0\frac{c_{111}}{c_{66}} + C_3^0\frac{c_{112}}{c_{66}} + C_4^0\frac{c_{123}}{c_{66}}) \\ & + S_h(C_1^{90} + C_2^{90}\frac{c_{111}}{c_{66}} + C_3^{90}\frac{c_{112}}{c_{66}} + C_4^{90}\frac{c_{123}}{c_{66}}),\end{aligned} \tag{25}$$

$$\begin{aligned}\frac{v_3 - v_R}{v_R} = \; & S_h(C_1^0 + C_2^0\frac{c_{111}}{c_{66}} + C_3^0\frac{c_{112}}{c_{66}} + C_4^0\frac{c_{123}}{c_{66}}) \\ & + S_H(C_1^{90} + C_2^{90}\frac{c_{111}}{c_{66}} + C_3^{90}\frac{c_{112}}{c_{66}} + C_4^{90}\frac{c_{123}}{c_{66}}),\end{aligned} \tag{26}$$

and

$$\frac{v^{St} - v_R^{St}}{v_R^{St}} = (S_H + S_h)(C_1 + C_2\frac{c_{111}}{c_{66}} + C_3\frac{c_{112}}{c_{66}} + C_4\frac{c_{123}}{c_{66}}), \tag{27}$$

where $v_R$ and $v_R^{St}$ are the flexural and Stoneley phase velocities in the reference state. Equations (25), (26) and (27) are used to estimate $S_H$, $S_h$, $c_{111}$, $c_{112}$, and $c_{123}$. Nonlinear constants $c_{111}$, $c_{112}$, and $c_{123}$ are not provided by the current logging technique. Therefore, we need to invert for them as well. In those equations, phase velocities of the Stoneley wave, $v^{St}$, and flexural waves, $v_2$ and $v_3$, can be estimated from the monopole and cross-dipole waveforms, respectively. Phase velocities in the reference state can be readily computed numerically by solving an eigenvalue problem of a fluid-filled borehole surrounded by an isotropic formation. Note that except for the five unknowns $S_H$, $S_h$, $c_{111}$, $c_{112}$, and $c_{123}$, and the formation elastic constant in the reference state $c_{66}$, all quantities in equations (25), (26) and (27) are frequency dependent. Consequently, multiple frequencies may be selected in order to have redundancy in the inversion.

## RESULTS FROM CROSS-DIPOLE AND MONOPOLE LOGS IN CALIFORNIA

Here, we analyze a set of cross-dipole and monopole waveforms acquired by a sonic tool in a vertical well for the estimation of formation stress directions and magnitudes. This well is located in a tectonically active area in California. Tectonic stresses can cause stress-induced shear anisotropy in such vertical wells. Our investigation of formation stresses consists of the following steps:

1. *Low-pass filtering and time windowing of cross-dipole waveforms.* First, we use a short Fourier transform, a technique that estimates time-localized frequency contents of a waveform and generates a time-frequency domain figure that is called a spectrogram, to analyze various wave modes generated in the borehole by dipole sources. Figure 1a shows a typical spectrogram of waveforms recorded by a cross-dipole log. Note the earliest arrival around 15 kHz is the tool mode followed by a compressional headwave around 5 kHz. The flexural mode is a high amplitude signal around 1.5 kHz with the lowest velocity around 600 m/s. Figure 1b shows velocities of all the modes in their respective frequency ranges. These results show the presence of a weak compressional mode around 5 kHz; a borehole flexural mode around 1.5 kHz; and a tool arrival around 15 kHz. Since a borehole flexural wave consists of low-frequency components and propagates the slowest among all the generated waves, low-pass filtering and time windowing the recorded waveforms help to obtain relatively pure flexural waves.

2. *Fast shear azimuth estimation and rotation of recorded dipole waveforms to the fast and slow shear directions.* The orientation of the fast shear or flexural wave polarization in the far field is obtained by using the low frequency part of cross-dipole flexural waveforms with the modified Alford rotation technique that takes into account the signature mismatch of sources and receivers (Huang *et al.*, 1998. Waveforms at each depth are then rotated so that the tool sources and receivers are aligned with the principal flexural wave polarizations. As a result, the rotated waveforms contain largely pure principal flexural waves and are ready for further processing.

3. *Dispersion analysis.* In order to locate depths where crossovers in flexural dispersions or stress-induced anisotropy occurs, flexural dispersions are extracted from the data using one mode method (Nolte *et al.*, 1997. Dipole dispersion crossover is continuously observed in the depth range of thickness 131 ft. Figure 2a presents a typical dispersion crossover for the two principal flexural waves in the aforementioned stressed zone. Figure 2b shows the compressional headwave and the dispersive Stoneley wave from monopole logging data in the same well at the same depth. The compressional wave velocity is around 1600 m/s, the same value presented in Figure 1 The presence of crossovers indicates horizontal formation stresses on a weakly anisotropic or isotropic formation at those depths where the polarization direction of the fast flexural wave corresponds to the direction of formation maximum horizontal stress. Figure 3 shows the maximum horizontal formation stress directions in the stressed zone. Additionally, by computing the cross-correlation of the low-frequency part of the fast and slow flexural waveforms, we obtain the group delays between the slow and fast flexural waves (Figure 3). The delays indicate the amount of stress-induced anisotropy in the formation. The sonic tool consists of a linear array of eight receiver stations with an inter-receiver spacing of 6 in. The dipole transmitter is located 11 ft from the nearest receiver.

The group delay is averaged over eight receivers. The distance $L$ from the transmitter to the mid-point of receiver array is 12.75 ft (3.886 m). The shear velocity anisotropy can be expressed as

$$\frac{V_2 - V_3}{V_3} = \frac{V_2 \Delta t}{L}, \tag{28}$$

where $V_2$ and $V_3$ are the fast and slow shear velocities, respectively; and $\Delta t$ is the group delay at a given depth as shown in the second panel of Figure 3. Typically, we observe a group delay $\Delta t$=1 ms, and an average shear velocity $V_2$=620 m/s (2034 ft/s) in this depth interval. These values yield an average shear anisotropy of about 16%. Note that the entire depth interval in Figure 3 shows dipole dispersion crossovers and a significant amount of stress-induced shear anisotropy. The maximum horizontal formation stress direction is oriented at $30^o$ to $50^o$ east from north.

4. *Stress magnitude estimation.* The dotted lines in Figure 4 represent dispersions measured from logs. From each of the dispersion curves of flexural waves and the Stoneley wave, five frequency points from the frequency band 1 kHz to 2 kHz with 250 Hz spacing are selected for inversion. Borehole properties that are used as the reference state in the inversion are listed below.

$$\begin{aligned}
\text{Formation compressional velocity} &: V_1 = 1693 m/s\,, \\
\text{Formation shear velocity} &: V_2 = 570 m/s\,, \\
\text{Formation mass density} &: \rho = 2400 kg/m^3\,, \\
\text{Borehole radius} &: R = 0.2 m\,, \\
\text{Fluid compressional velocity} &: V_f = 1500 m/s\,, \\
\text{Fluid mass density} &: \rho_f = 1000 kg/m^3.
\end{aligned}$$

Magnitudes of the maximum and minimum horizontal formation stresses as well as three formation nonlinear elastic constants are inverted using equations (25), (26) and (27). The results are as follows:

$$\begin{aligned}
S_H = -40 MPa\,, \quad S_h = -12 MPa\,, \\
c_{111} = -608.6 GPa\,, \quad c_{112} = 25.4 GPa\,, \\
c_{123} = 201.2 GPa.
\end{aligned}$$

Theoretical dispersion curves are calculated by substituting the estimation results back to equations (25), (26) and (27). Agreement between measured and theoretical dispersion curves indicates very small mean-square errors of the inversion.

From the dispersion curves of flexural waves (Figure 4), it is obvious that the formation of the well is very soft, i.e., with very low shear velocity, around 610 $m/s$. As the formation mass density is about average, around 2300 $kg/m^3$, we

may conclude that the shear modulus, and thus shear stress, is relatively small in the formation. Therefore, formation overburden can be a good approximation of the vertical stress, $S_v$. Assuming that the average formation density from the surface to the depth of 400 m is 2300 $kg/m^3$, the vertical stress in the depth range of the stressed zone is on the order of 8.8 to 9.7 $MPa$ , and this magnitude is comparable with $S_h$. Consequently, the stress field of the studied area is of the form $S_H \gg S_h \approx S_v$, producing a combination of strike-slip and thrust faulting. These results are consistent with results from borehole breakout studies (Mount and Suppe, 1992), and with focal mechanism and borehole breakout data presented in the world stress map database (Zoback, 1992).

## DISCUSSION

The existence of a borehole alters the stress field in the formation. The stress field distribution around a borehole caused by a far-field compressive stress $S$ is given by Timoshenko and Goodier (1982)

$$\begin{aligned}
T_{RR} &= \frac{S}{2}(1-\frac{a^2}{R^2})+\frac{S}{2}(1+\frac{3a^4}{R^4}-\frac{4a^2}{R^2})cos2\Phi\,,\\
T_{\Phi\Phi} &= \frac{S}{2}(1+\frac{a^2}{R^2})-\frac{S}{2}(1+\frac{3a^4}{R^4})cos2\Phi\,,\\
T_{R\Phi} &= -\frac{S}{2}(1-\frac{3a^4}{R^4}+\frac{2a^2}{R^2})sin2\Phi\,,\\
T_{ZZ} &= \mu(T_{RR}+T_{\Phi\Phi})\,,\\
T_{ZR} &= 0\,,\\
T_{Z\Phi} &= 0
\end{aligned} \tag{29}$$

where $a$ is borehole radius, $\mu$ is the formation Poisson's ratio, $R$ is the radial distance from the borehole axis, and $\Phi$ is the azimuth angle that is measured relative to the far-field uniaxial stress direction. Figure 5 shows radial ($T_{RR}$), circumferential($T_{\Phi\Phi}$) and radial-azimuthal shear ($T_{R\Phi}$) stress variations away from the borehole surface along various azimuthal directions from the stress axis ($\Phi = 0^o, 30^o, 60^o$, and $90^o$). All stresses are normalized with respect to the far-field stress, S. When the radial distance, $R$ is over two to three times the borehole radius, the stress field is very close to that of the far-field. Borehole guided waves can efficiently penetrate the formation to the radial distance of one wavelength (Cheng and Toksöz, 1981). The center frequency of Stoneley and borehole flexural waves that are used in the stress magnitude inversion is 1 kHz. Velocities of Stoneley wave and both flexural waves are over 600 m/s. Therefore, Stoneley wave and flexural waves are sensitive to formation properties up to 60 cm from the center of the borehole, or over three times of the borehole radius. Therefore, the estimated stress magnitudes represent the far-field formation stress quite well.

## CONCLUSIONS

Techniques presented in this paper for studying *in situ* formation stresses are nondestructive, require no extra measurement, as they make use of the standard acoustic logging data, and are reasonably reliable in estimating absolute stress magnitudes. Inversions for stress directions and magnitudes are simple, efficient and, moreover, well-conditioned.

Anisotropy in rocks can be characterized as either intrinsic or stress-induced. It is possible to have a mixture of these two types of anisotropy in the earth. The stress magnitude inversion scheme presented in this paper requires observations of stress-induced anisotropy dominating intrinsic anisotropy. When intrinsic anisotropy is comparable to stress-induced anisotropy throughout the borehole, the current technique may not give accurate results.

## ACKNOWLEDGMENTS

This work was supported by the Borehole Acoustics and Logging/Reservoir Delineation Consortia at the Massachusetts Institute of Technology. Special thanks to Chevron Petroleum Technology Company for providing us with well logs.

## REFERENCES

Biot, M.A., 1952, Propagation of elastic waves in a cylindrical bore containing a fluid, *J. Appl. Phys., 23*, 997–1005.

Cheng, C.H. and Toksöz, M.N., 1981, Elastic wave propagation in a fluid-filled borehole and synthetic acoustic logs, *Geophysics, 46*, 1042–1053.

Gough, D.I. and Bell, R.S., 1982, Stress orientations from borehole wall fractures with examples from Colorado, east Texas, and northern Canada, *Can. J. Earth Sci., 19*, 1358–1370.

Huang, X., Burns, D.R., and Toksöz, M.N., 1998, Dispersion analysis of cross-dipole data, *Borehole Acoustics and Logging/Reservoir Delineation Consortia Annual Report, MIT* .

Mount, V.S. and Suppe, J., 1992, Present-day stress orientations adjacent to active strike-slip faults: California and Sumatra, *J. Geophys. Res., 97*, 11,995–12,013.

Nolte, B., Rao, R., and Huang, X., 1997, Dispersion analysis of split flexural waves, *Borehole Acoustics and Logging/Reservoir Delineation Consortia Annual Report, MIT* .

Norris, A.N., Bikash, K.S., and Kostek, S., 1994, Acoustoelasticity of solid/fluid composite systems, *Geophys. J. Int., 118*, 439–446.

Sinha, B.K., 1997, Inversion of borehole dispersions for formation stresses, *Proc. 1997 IEEE International Ultrasonic Symposium, October 5–8, IEEE Catalog No. 97CH36118*, pp. 781–786.

Sinha, B.K. and Kostek, S., 1996, Stress-induced azimuthal anisotropy in borehole flexural waves, *Geophysics, 61*, 1899–1907.

Thurston, R.N. and Brugger, K., 1964, Third-order elastic constants and the velocity of small amplitude elastic waves in homogeneously stressed media, *Phys. Rev., 33*, A1604–1610.

Tiersten, H.F., 1978, Perturbation theory for linear electroelastic equations for small fields superposed on a bias, *J. Acoust. Soc. Am., 64*, 832–837.

Timoshenko, S.P. and Goodier, J.N., 1982, *Theory of Elasticity*, McGraw Hill Book Co.

Truesdell, C. and Noll, W., 1992, *The Nonlinear Field Theories of Mechanics*, New York.

Winkler, K.W., Sinha, B.K., and Plona, T.J., 1998, Effects of borehole stress concentrations on dipole anisotropy measurements, *Geophysics, 63*, 11–17.

Zoback, M.D., Moos, D., and Anderson, R.N., 1985, Wellbore breakouts and in situ stress, *J. Geophys. Res., 90*, 5523–5530.

Zoback, M.L., 1992, First- and second-order patterns of stress in the lithosphere: the world stress map project, *J. Geophys. Res., 97*, 11,703–11,728.

Zoback, M.L. and Zoback, M.D., 1980, State of stress of the conterminous United States, *J. Geophys. Res., 85*, 6113–6156.

# APPENDIX

## Sensitivity Coefficients for Flexural Dispersions to the Formation Stress and Nonlinear Constants

The sensitivity coefficients $C_1^0$, $C_2^0$, $C_3^0$, $C_4^0$, are given by the following integrals

$$C_1^0 = \frac{I_1}{2\omega_m^2 I_N}, \tag{A-1}$$

$$C_2^0 = \frac{c_{66} I_2}{2\omega_m^2 I_N}, \tag{A-2}$$

$$C_3^0 = \frac{c_{66} I_3}{2\omega_m^2 I_N}, \tag{A-3}$$

$$C_4^0 = \frac{c_{66} I_4}{2\omega_m^2 I_N}. \tag{A-4}$$

Since the integral $I_1$ consists of several lengthy expressions, we express this integral as a sum of 9 terms as shown below:

$$I_1 = \sum_{Q=1}^{9} I_{1Q}, \tag{A-5}$$

where

$$\begin{aligned} I_{11} &= \int_a^\infty r dr \int_0^{2\pi} d\phi [T_{ZZ} u_{z,z} + c_{12}[E_{RR} u_{r,r} + E_{\Phi\Phi}(\frac{u_{\phi,\phi}}{r} + \frac{u_r}{r})] \\ &+ c_{12} E_{R\Phi}(\frac{u_{r,\phi}}{r} - \frac{u_\phi}{r} + u_{\phi,r})] u^*_{z,z}, \end{aligned} \tag{A-6}$$

$$\begin{aligned} I_{12} &= \int_a^\infty r dr \int_0^{2\pi} d\phi [c_{12} E_{RR} u_{z,z} + 2c_{11} E_{RR} u_{r,r} + T_{RR} u_{r,r} \\ &+ c_{12}(E_{RR} + E_{\Phi\Phi})(\frac{u_{\phi,\phi}}{r} + \frac{u_r}{r}) + c_{66} E_{RZ}(\frac{u_{r,\phi}}{r} - \frac{u_\phi}{r} + u_{\phi,r}) \\ &+ (T_{R\Phi} + c_{12} E_{R\Phi}) u_{r,\phi} + c_{11} E_{R\Phi} u_{\phi,r}] u^*_{r,r}, \end{aligned} \tag{A-7}$$

$$\begin{aligned} I_{13} &= \int_a^\infty r dr \int_0^{2\pi} d\phi [c_{12} E_{\Phi\Phi} u_{z,z} + c_{12}(E_{RR} + E_{\Phi\Phi}) u_{r,r} \\ &+ (2c_{11} E_{\Phi\Phi} + T_{\Phi\Phi})(\frac{u_{\phi,\phi}}{r} + \frac{u_r}{r}) + c_{66} E_{R\Phi}(\frac{u_{r,\phi}}{r} - \frac{u_\phi}{r} + u_{\phi,r}) \\ &+ (T_{R\Phi} + c_{12} E_{R\Phi}) u_{\phi,r} + c_{11} E_{R\Phi}(\frac{u_{r,\phi}}{r} - \frac{u_\phi}{r})](\frac{u^*_{\phi,\phi}}{r} + \frac{u^*_r}{r}), \end{aligned} \tag{A-8}$$

$$I_{14} = \int_a^\infty r dr \int_0^{2\pi} d\phi [T_{RR} u_{z,r} + T_{R\Phi} \frac{u_{z,\phi}}{r} + c_{66}(E_{RR} u_{r,z} + E_{R\Phi} u_{\phi,z})] u^*_{z,r}, \tag{A-9}$$

$$I_{15} = \int_a^\infty r dr \int_0^{2\pi} d\phi [c_{66} E_{RR}(u_{z,r} + u_{r,z}) + c_{66} E_{R\Phi}(\frac{u_{z,\phi}}{r} + u_{\phi,z}) + (T_{ZZ} + c_{66} E_{RR}) u_{r,z} + c_{66} E_{R\Phi} u_{\phi,z}] u^*_{r,z}\,, \quad \text{(A-10)}$$

$$I_{16} = \int_a^\infty r dr \int_0^{2\pi} d\phi [T_{ZZ} u_{\phi,z} + c_{66}(E_{R\Phi} u_{r,z} + E_{\Phi\Phi} u_{\phi,z}) + c_{66} E_{R\Phi}(u_{z,r} + u_{r,z}) + c_{66} E_{\Phi\Phi}(\frac{u_{z,\phi}}{r} + u_{\phi,z})] u^*_{\phi,z}\,, \quad \text{(A-11)}$$

$$I_{17} = \int_a^\infty r dr \int_0^{2\pi} d\phi [T_{R\Phi} u_{z,r} + T_{\Phi\Phi} \frac{u_{z,\phi}}{r} + c_{66}(E_{R\Phi} u_{r,z} + E_{\Phi\Phi} u_{\phi,z})] \frac{u^*_{z,\phi}}{r}\,, \quad \text{(A-12)}$$

$$I_{18} = \int_a^\infty r dr \int_0^{2\pi} d\phi [c_{12} E_{R\Phi} u_{z,z} + (c_{11} + c_{66}) E_{R\Phi} u_{r,r} + c_{66} E_{RR}(\frac{u_{r,\phi}}{r} - \frac{u_\phi}{r}) + (T_{R\Phi} + (c_{66} + c_{12}) E_{R\Phi})(\frac{u_{\phi,\phi}}{r} + \frac{u_r}{r}) + (T_{RR} + c_{66} E_{\Phi\Phi}) u_{\phi,r} + c_{66} E_{\Phi\Phi}(\frac{u_{r,\phi}}{r} - \frac{u_\phi}{r} + u_{\phi,r})] u^*_{\phi,r}\,, \quad \text{(A-13)}$$

$$I_{19} = \int_a^\infty r dr \int_0^{2\pi} d\phi [c_{12} E_{R\Phi} u_{z,z} + (c_{11} + c_{66}) E_{R\Phi}(\frac{u_{\phi,\phi}}{r} + \frac{u_r}{r}) + c_{66} E_{\Phi\Phi} u_{\phi,r} + (T_{R\Phi} + (c_{66} + c_{12}) E_{R\Phi}) u_{r,r} + (T_{\Phi\Phi} + c_{66} E_{RR})(\frac{u_{r,\phi}}{r} - \frac{u_\phi}{r}) + c_{66} E_{RR}(\frac{u_{r,\phi}}{r} - \frac{u_\phi}{r} + u_{\phi,r})](\frac{u^*_{r,\phi}}{r} - \frac{u^*_\phi}{r}). \quad \text{(A-14)}$$

The remaining integrals $I_2$, $I_3$, $I_4$ and $I_N$ take the following forms

$$I_2 = \int_a^\infty r dr \int_0^{2\pi} d\phi [[E_{RR} u_{r,r} + \frac{1}{2} E_{R\Phi}(\frac{u_{r,\phi}}{r} - \frac{u_\phi}{r} + u_{\phi,r})] u^*_{r,r} + [E_{\Phi\Phi} u_{\phi,\phi} + \frac{1}{2} E_{R\Phi}(\frac{u_{r,\phi}}{r} - \frac{u_\phi}{r} + u_{\phi,r})](\frac{u^*_{\phi,\phi}}{r} + \frac{u^*_r}{r}) + \frac{1}{4}[E_{RR}(u_{r,z} + u_{z,r}) + E_{R\Phi}(\frac{u_{z,\phi}}{r} + u_{\phi,z})](u^*_{z,r} + u^*_{r,z}) + \frac{1}{4}[E_{R\Phi}(u_{r,z} + u_{z,r}) + E_{\Phi\Phi}(\frac{u_{z,\phi}}{r} + u_{\phi,z})](u^*_{\phi,z} + \frac{u^*_{z,\phi}}{r}) + \frac{1}{4}[(E_{RR} + E_{\Phi\Phi})(\frac{u_{r,\phi}}{r} - \frac{u_\phi}{r} + u_{\phi,r}) + 2E_{R\Phi}(u_{r,r} + \frac{u_{\phi,\phi}}{r} + \frac{u_r}{r})](u^*_{\phi,r} + u^*_{r,\phi})]\,, \quad \text{(A-15)}$$

$$I_3 = \int_a^\infty r dr \int_0^{2\pi} d\phi [[(E_{RR} + E_{\Phi\Phi}) u_{z,z} + E_{RR} u_{r,r} + E_{\Phi\Phi}(\frac{u_{\phi,\phi}}{r} + \frac{u_r}{r}) + E_{R\Phi}(\frac{u_{r,\phi}}{r} - \frac{u_\phi}{r} + u_{\phi,r})] u^*_{z,z} + [E_{RR} u_{z,z} + E_{\Phi\Phi} u_{r,r} + (E_{RR} + E_{\Phi\Phi})(\frac{u_{\phi,\phi}}{r} + \frac{u_r}{r}) -$$

$$
\begin{aligned}
& \frac{1}{2}E_{R\Phi}\left(\frac{u_{r,\phi}}{r}-\frac{u_\phi}{r}+u_{\phi,r}\right)]u^*_{r,r} \\
+ \; & [E_{\Phi\Phi}u_{z,z}+(E_{RR}+E_{\Phi\Phi})u_{r,r}+E_{RR}\left(\frac{u_{\phi,\phi}}{r}+\frac{u_r}{r}\right)- \\
& \frac{1}{2}E_{R\Phi}\left(\frac{u_{r,\phi}}{r}-\frac{u_\phi}{r}+u_{\phi,r}\right)]\left(\frac{u^*_{\phi,\phi}}{r}+\frac{u^*_r}{r}\right) \\
+ \; & \frac{1}{4}[(2E_{\Phi\Phi}-E_{RR})(u_{r,z}+u_{z,r})-3E_{R\Phi}\left(\frac{u_{z,\phi}}{r}+u_{\phi,z}\right)](u^*_{z,r}+u^*_{r,z}) \\
+ \; & \frac{1}{4}[(2E_{RR}-E_{\Phi\Phi})\left(\frac{u_{z,\phi}}{r}+u_{\phi,z}\right)-3E_{R\Phi}(u_{z,r}+u_{r,z})](u^*_{\phi,z}+u^*_{z,\phi}) \\
+ \; & \frac{1}{2}(2E_{R\Phi}u_{z,z}-E_{R\Phi})(u_{r,r}+\frac{u_{\phi,\phi}}{r}+\frac{u_r}{r})(u^*_{\phi,r}+u^*_{r,\phi}) \\
- \; & \frac{1}{2}(E_{RR}+E_{\Phi\Phi})\left(\frac{u_{r,\phi}}{r}-\frac{u_\phi}{r}+u_{\phi,r}\right)(u^*_{\phi,r}+u^*_{r,\phi})]\,, \qquad \text{(A-16)}
\end{aligned}
$$

$$
\begin{aligned}
I_4 \; = \; & \int_a^\infty r\,dr\int_0^{2\pi}d\phi[[E_{\Phi\Phi}u_{r,r}+E_{RR}\left(\frac{u_{\phi,\phi}}{r}+\frac{u_r}{r}\right)-E_{R\Phi}\left(\frac{u_{r,\phi}}{r}-\frac{u_\phi}{r}+u_{\phi,r}\right)]u^*_{z,z} \\
+ \; & E_{\Phi\Phi}u_{z,z}u^*_{r,r}+E_{RR}u_{z,z}\left(\frac{u^*_{\phi,\phi}}{r}+\frac{u^*_r}{r}\right) \\
+ \; & \frac{1}{2}[E_{R\Phi}\left(\frac{u_{z,\phi}}{r}+u_{\phi,z}\right)-E_{\Phi\Phi}(u_{z,r}+u_{r,z})](u^*_{z,r}+u^*_{r,z}) \\
+ \; & \frac{1}{2}[E_{R\Phi}(u_{r,z}+u_{z,r})-E_{RR}\left(\frac{u_{z,\phi}}{r}+u_{\phi,z}\right)](u^*_{\phi,z}+u^*_{z,\phi}) \\
- \; & E_{R\Phi}u_{z,z}(u^*_{\phi,r}+\frac{u^*_{r,\phi}}{r}-\frac{u^*_\phi}{r})]\,, \qquad \text{(A-17)}
\end{aligned}
$$

$$
\begin{aligned}
I_N \; = \; & \int_0^a r\,dr\int_0^{2\pi}d\phi\rho_f[u^f_r u^{f*}_r+u^f_\phi u^{f*}_\phi+u^f_z u^{f*}_z] \\
+ \; & \int_a^\infty r\,dr\int_0^{2\pi}d\phi\rho_s[u_r u^*_r+u_\phi u^*_\phi+u_z u^*_z]\,, \qquad \text{(A-18)}
\end{aligned}
$$

where $T_{ZZ}$ is the axial stress in the formation; $E_{RR}$, $E_{\Phi\Phi}$ and $E_{R\Phi}$ are the static strains in the formation written in the cylindrical-polar coordinates; $c_{11}$, $c_{12}$ and $c_{66}$ are the linear elastic constants of the formation in the reference state; $u^f_r$, $u^f_\phi$ and $u^f_z$ denote flexural wave solutions in the fluid; and, $u_r$, $u_\phi$ and $u_z$ are flexural wave solutions in the formation with radial polarization parallel to the far-field stress direction.

The sensitivity coefficients $C^{90}_1$, $C^{90}_2$, $C^{90}_3$ and $C^{90}_4$ are given by the same expressions as for $C^0_1$, $C^0_2$, $C^0_3$ and $C^0_4$, except for the important difference that all of the biasing stresses and strains are rotated by $90^o$ from before so that the far-field stress direction is now perpendicular to the flexural wave radial polarization direction.

## Sensitivity Coefficients for the Stoneley Dispersion to the Formation Stress and Nonlinear Constants

The sensitivity coefficients $C_1$, $C_2$, $C_3$ and $C_4$ are given by the following integrals

$$C_1 = \frac{J_1}{2\omega_m^2 J_N}, \tag{A-19}$$

$$C_2 = \frac{c_{66} J_2}{2\omega_m^2 J_N}, \tag{A-20}$$

$$C_3 = \frac{c_{66} J_3}{2\omega_m^2 J_N}, \tag{A-21}$$

$$C_4 = \frac{c_{66} J_4}{2\omega_m^2 J_N} \tag{A-22}$$

where $J_1$, $J_2$, $J_3$ and $J_4$ are expressed in terms of surface integrals as shown below:

$$\begin{aligned} J_1 &= \int_a^\infty r dr \int_0^{2\pi} d\phi [[T_{ZZ} u_{z,z} + c_{12}(E_{RR} u_{r,r} + E_{\Phi\Phi}\frac{u_r}{r})] u^*_{z,z} \\ &+ [c_{12} E_{RR} u_{z,z} + (T_{RR} + 2c_{11} E_{RR}) u_{r,r} + c_{12}(E_{RR} + E_{\Phi\Phi})\frac{u_r}{r}] u^*_{r,r} \\ &+ [c_{12} E_{\Phi\Phi} u_{z,z} + (T_{\Phi\Phi} + 2c_{11} E_{\Phi\Phi})\frac{u_r}{r} + c_{12}(E_{RR} + E_{\Phi\Phi}) u_{r,r}]\frac{u^*_r}{r} \\ &+ [T_{RR} u_{z,r} + c_{66} E_{RR} u_{r,z}] u^*_{z,r} \\ &+ [c_{66} E_{RR}(u_{z,r} + u_{r,z}) + (T_{ZZ} + c_{66} E_{RR}) u_{r,z}] u^*_{r,z}], \end{aligned} \tag{A-23}$$

$$\begin{aligned} J_2 &= \int_a^\infty r dr \int_0^{2\pi} d\phi [[E_{RR} u_{r,r}] u^*_{r,r} + [E_{\Phi\Phi}\frac{u_r}{r}]\frac{u^*_r}{r} \\ &+ \frac{1}{4}[E_{RR}(u_{z,r} + u_{r,z})](u^*_{z,r} + u^*_{r,z})], \end{aligned} \tag{A-24}$$

$$\begin{aligned} J_3 &= \int_a^\infty r dr \int_0^{2\pi} d\phi [[E_{RR} + E_{\Phi\Phi}) u_{z,z} + E_{\Phi\Phi}\frac{u_r}{r} + E_{RR} u_{r,r}] u^*_{z,z} \\ &+ [E_{RR} u_{z,z} + E_{\Phi\Phi} u_{r,r} + (E_{RR} + E_{\Phi\Phi})\frac{u_r}{r}] u^*_{r,r} \\ &+ [E_{\Phi\Phi} u_{z,z} + E_{RR}\frac{u_r}{r} + (E_{RR} + E_{\Phi\Phi}) u_{r,r}]\frac{u^*_r}{r} \\ &+ \frac{1}{4}[(2E_{\Phi\Phi} - E_{RR})(u_{z,r} + u_{r,z})](u^*_{z,r} + u^*_{r,z})], \end{aligned} \tag{A-25}$$

$$\begin{aligned} J_4 &= \int_a^\infty r dr \int_0^{2\pi} d\phi [[E_{\Phi\Phi} u_{r,r} + E_{RR}\frac{u_r}{r}] u^*_{z,z} \\ &+ E_{\Phi\Phi} u_{z,z} u^*_{r,r} + E_{RR} u_{z,z}\frac{u^*_r}{r} \\ &- \frac{1}{2}[E_{\Phi\Phi}(u_{z,r} + u_{r,z})](u^*_{z,r} + u^*_{r,z})], \end{aligned} \tag{A-26}$$

$$J_N = \int_0^a r dr \int_0^{2\pi} d\phi \rho_f (u_r^f u_r^{f*} + u_z^f u_z^{f*}) + \int_a^\infty r dr \int_0^{2\pi} d\phi \rho_s (u_r u_r^* + u_z u_z^*), \quad \text{(A-27)}$$

where $u_r^f$ and $u_z^f$ denote the Stoneley wave solution in the borehole fluid; and, $u_r$ and $u_z$ are the corresponding solution in the formation.

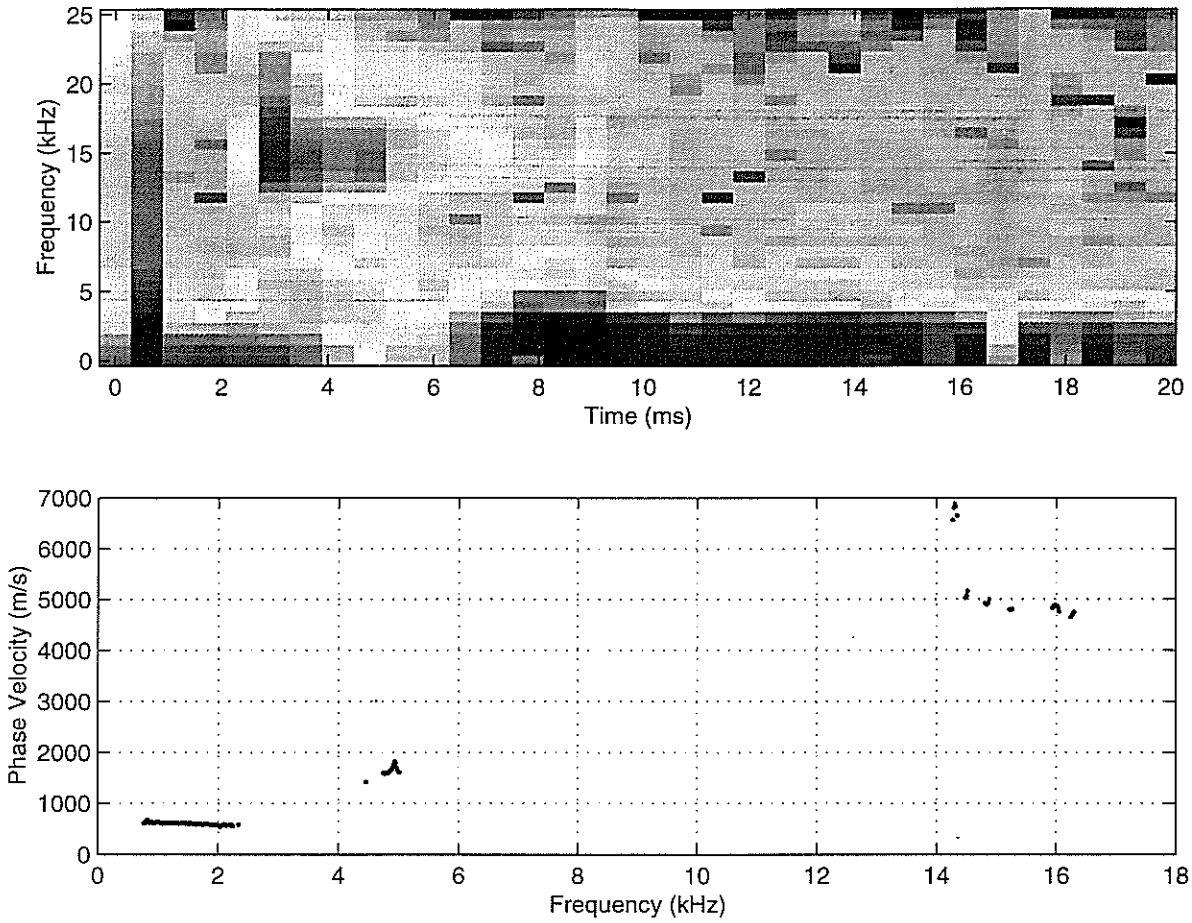


Figure 1: Separation of all borehole modes that are generated by the sonic tool. (a, top): A typical spectrogram of recorded waveforms. Red and blue colors indicate high and low amplitudes of signals in the measurement frequency band of approximately 1 to 20 kHz. (b, bottom): Velocities and frequency band of the flexural mode, compressional headwave, and a first-order tool mode.

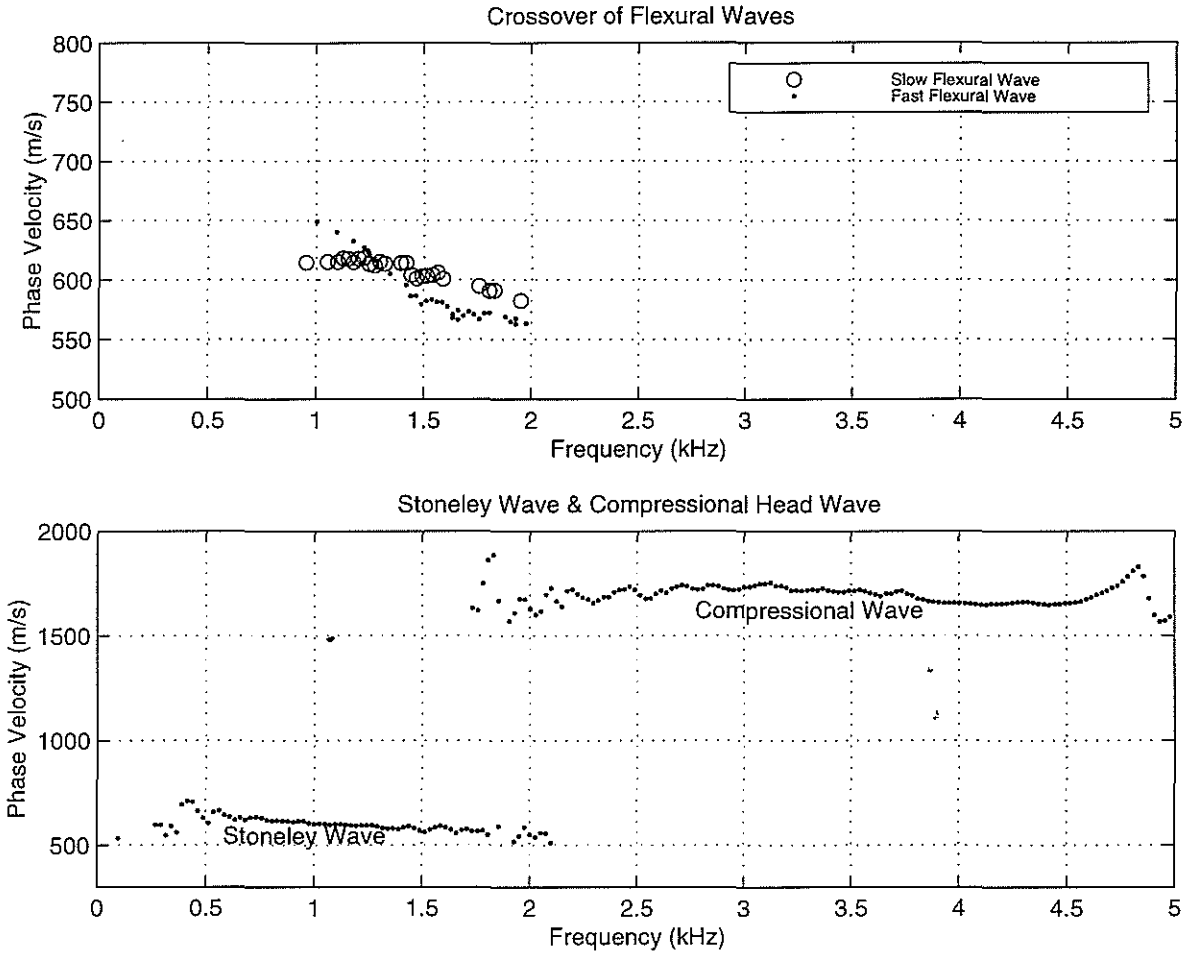


Figure 2: Typical dispersion curves of borehole modes in the stressed zone extracted from the sonic logging data. (a, top): Flexural waves from cross-dipole logging; (b, bottom): Compressional headwave and Stoneley wave from monopole logging.

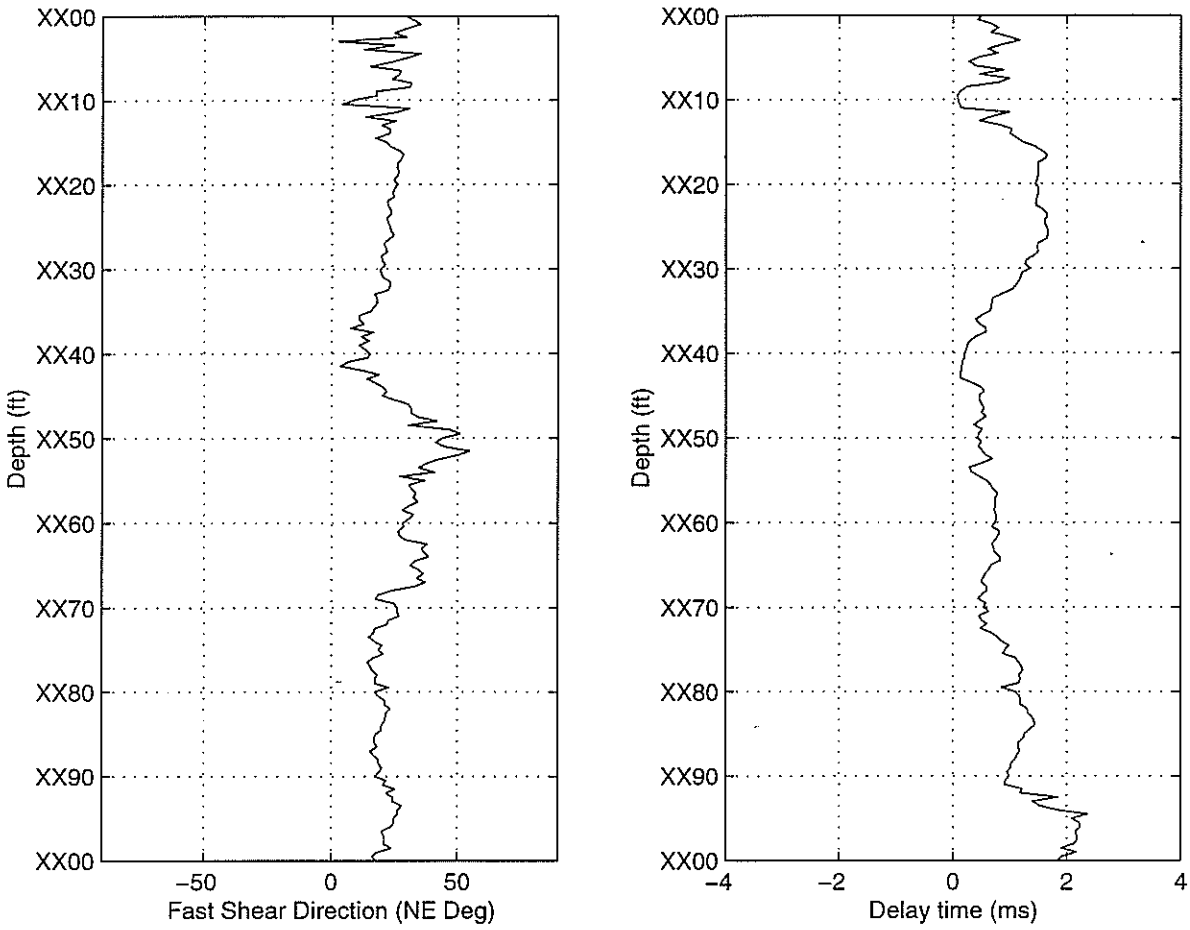


Figure 3: Maximum stress direction in the stressed zone where crossovers in flexural dispersions are continuously observed. The second panel shows the group delay of the slow flexural wave from the fast one by cross-correlating the low-frequency part of the fast and slow flexural waveforms, indicating the amount of anisotropy that the stress induces in the formation.

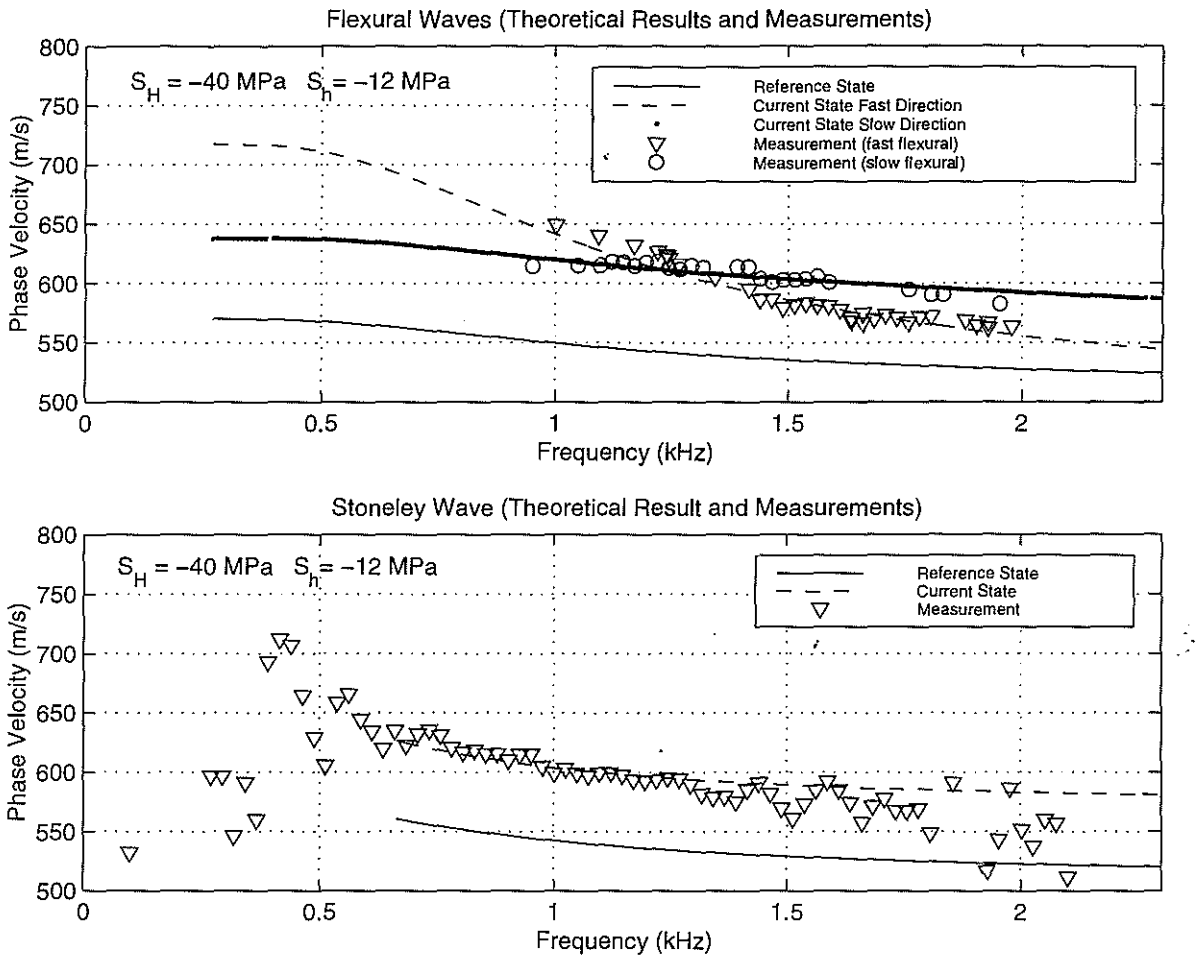


Figure 4: Dispersion curves that are estimated from data as well as calculated by the perturbation theory with inverted tectonic stresses and nonlinear elastic constants as inputs.

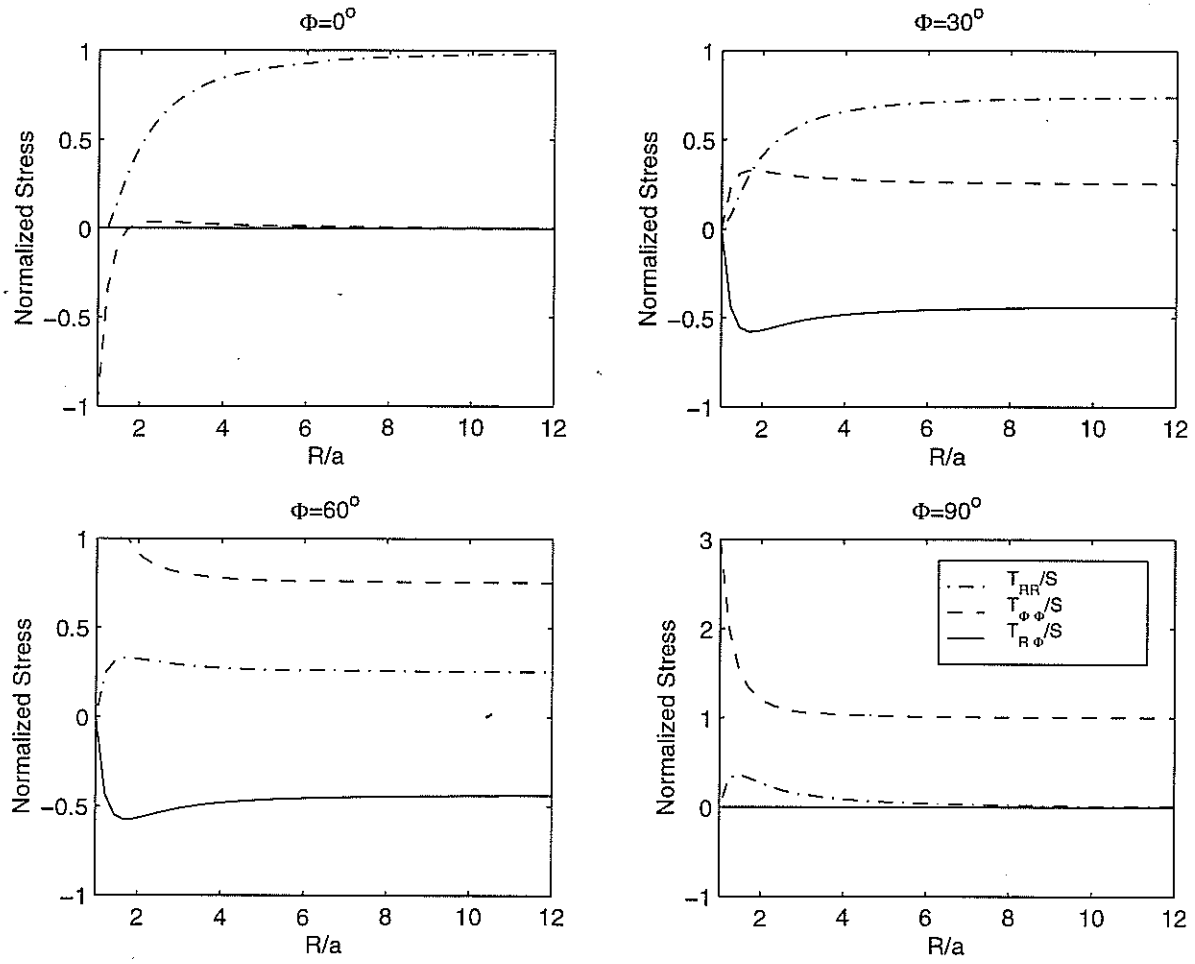


Figure 5: Radial ($T_{RR}$), circumferential($T_{\Phi\Phi}$) and radial-azimuthal shear ($T_{R\Phi}$) stress variations away from the borehole surface along various azimuthal directions from the stress axis ($\Phi = 0^o, 30^o, 60^o$, and $90^o$). All stresses are normalized with respect to the far-field stress S.